Age-Related Retinal Changes in Wild-Type C57BL/6J Mice Between 2 and 32 Months

Salma Ferdous,[1] Kristie L. Liao,[1] Isabelle D. Gefke,[1] Vivian R. Summers,[1] Wenfei Wu,[1,2] Kevin J. Donaldson,[1] Yong-Kyu Kim,[1,3] Jana T. Sellers,[1] Jendayi A. Dixon,[1] Debresha A. Shelton,[1] Shanu Markand,[1] Somin M. Kim,[1] Nan Zhang,[1,4] Jeffrey H. Boatright,[1,5] and John M. Nickerson[1]

[1]Department of Ophthalmology, Emory University, Atlanta, Georgia, United States
[2]The First Affiliated Hospital of Medical School of Xi'an Jiaotong University, Xi'an, Shan'xi, China
[3]Department of Ophthalmology, Hallym University College of Medicine, Kangdong Sacred Heart Hospital, Gangdong-gu, Seoul, South Korea
[4]Department of Ophthalmology, Second Xiangya Hospital of Central South University, Changsha, Hunan, China
[5]Atlanta Veterans Administration Center for Visual and Neurocognitive Rehabilitation, Decatur, Georgia, United States

Correspondence: John M. Nickerson, Department of Ophthalmology, Room B5602, Emory University, 1365B Clifton Road, NE, Atlanta, GA 30322, USA; litjn@emory.edu.

Received: October 7, 2020
Accepted: April 21, 2021
Published: June 8, 2021

Citation: Ferdous S, Liao KL, Gefke ID, et al. Age-related retinal changes in wild-type C57BL/6J mice between 2 and 32 months. *Invest Ophthalmol Vis Sci*. 2021;62(7):9. https://doi.org/10.1167/iovs.62.7.9

Purpose. The purpose of this study was to extend our understanding of how aging affects normal retina function and morphology in wild-type C57BL/6J mice, by analyzing electrophysiological recordings and *in vivo* and post mortem anatomy.

Methods. Electroretinograms (ERGs), spectral domain optical coherence tomography (SD-OCT), and confocal scanning laser ophthalmoscope (cSLO) *in vivo* images were obtained from mice between the ages of 2 and 32 months in four groups: group 1 (<0.5 years), group 2 (1.0–1.5 years), group 3 (1.5–2.0 years), and group 4 (>2.0 years). Afterward, mouse bodies and eyes were weighed. Eyes were stained with hematoxylin and eosin (H&E) and cell nuclei were quantified.

Results. With aging, mice showed a significant reduction in both a- and b-wave ERG amplitudes in scotopic and photopic conditions. Additionally, total retina and outer nuclear layer (ONL) thickness, as measured by SD-OCT images, were significantly reduced in older groups. The cSLO images showed an increase in auto-fluorescence at the photoreceptor-RPE interface as age increases. H&E cell nuclei quantification showed significant reduction in the ONL in older ages, but no differences in the inner nuclear layer (INL) or ganglion cell layer (GCL).

Conclusions. By using multiple age groups and extending the upper age limit of our animals to approximately 2.65 years (P970), we found that natural aging causes negative effects on retinal function and morphology in a gradual, rather than abrupt, process. Future studies should investigate the exact mechanisms that contribute to these gradual declines in order to discover pathways that could potentially serve as therapeutic targets.

Keywords: aging, retina, mouse, C57BL/6J

Age-related visual impairment affects the physical, psychological, and social function of older adults[1] and is a major risk factor for many prevalent ophthalmic disorders.[2] Even healthy patients have structural retinal changes with age, including decreased retinal nerve fiber layer and mean central retinal thickness,[3] as well as decreased thickness of individual retinal layers, such as the ganglion cell layer (GCL), inner plexiform layer (IPL), and inner nuclear layer (INL).[4] These changes in retinal layer thickness are accompanied by decreased rod photoreceptor density,[5] altered retinal microvasculature,[6,7] mitochondrial dysfunction with increased reactive oxygen species (ROS) generation,[8] and para-inflammation.[9] The morphological and physiological changes likely cause exponential decreases in rod and cone amplitudes and increased implicit times in both photopic and scotopic conditions.[10,11] Outside of the retina, aging can cause stiffening of lens fibers and zonules, leading to presbyopia, and the loss of transparency in lens crystallin, leading to cataracts.[2] Additionally, as age increases, macrophages and microglia infiltrate the photoreceptor-retinal pigment epithelium (RPE) interface,[12,13] there is an increase in intracellular lipofuscin and extracellular drusen,[14,15] and Bruch's membrane thickens.[16]

Animal studies evaluating age-related changes in the visual system have observed gross structural, morphological, and functional changes in both the retina and RPE and explored underlying mechanisms. Aging studies in rats showed gradual decreases in a- and b-wave electroretinogram (ERG) responses and significant thinning was observed in the IPL, outer plexiform layer (OPL), INL, and outer nuclear layer (ONL).[17,18] In mice, similar decreases in ERG responses were observed between 1.5 and 18 months of

age, which correlated with metabolic changes in the retina, RPE/choroid, optic nerve, and lens.[19]

Many aging studies in rodents compare relatively young animals (< 6 months) to "aged" animals, which range from roughly 1 to 2 years old. Although useful as a general comparison, investigating the differences between 1 "young" group and 1 "aged" group does not provide information on the overall progression of ocular changes due to aging. Therefore, we included multiple age groups in our current study to identify a general age when these ocular changes occur as well as extend the upper age limit to include animals that are at the maximum life expectancy of mice. The purpose of this study was to build upon and extend our understanding of how aging affects normal retina function and morphology by analyzing electrophysiological recordings and *in vivo* and post mortem anatomic data collected from wild-type C57BL/6J animals aged 2 to 32 months.

Methods

Animals

Mouse housing, experiments, and handling were approved by the Emory University Institutional Animal Care and Use Committee. Studies were conducted in adherence with Association for Research in Vision and Ophthalmology (ARVO) and followed guidance and principles of the Association for Assessment and Accreditation of Laboratory Animal Care (AAALAC). C57BL/6J (wild-type) mice were maintained on a 12-hour light/dark cycle at 22°, and standard mouse chow (Lab Diet 5001; PMI Nutrition Inc., LLC, Brentwood, MO, USA) and water were provided ad libitum. Animals were either purchased from Jackson Laboratories (JAX) directly or bred in-house for three generations or less from JAX breeding pairs. The mice in each group represent multiple different litters and all of the mice used in this study are independent from one another (i.e. no mouse was included in multiple groups). Therefore, we expect no batch effects. The mice were managed and housed by Emory University Division of Animal Resources. Adult mice were euthanized using CO_2 gas asphyxiation for 5 minutes followed by cervical dislocation. All mice used for this study were divided up into the following groups: group 1 (postnatal day 60–180); group 2 (postnatal day 365–544); group 3 (postnatal day 545–729); and group 4 (postnatal day 730+). There is a fair distribution of genders in all groups (see the Table).

Electroretinograms

Mice were dark-adapted overnight the day before ERGs were assessed. Each mouse was anesthetized using intraperitoneal (IP) injections of 100 mg/kg of ketamine and 15 mg/kg xylazine (ketamine; KetaVed from Patterson Veterinary, Greeley, CO, USA; xylazine from Patterson Veterinary).

Once anesthetized, proparacaine (1%; Akorn Inc., Ann Arbor, MI, USA) and tropicamide (1%; Akorn Inc.) eye drops were administered as a topical anesthetic and to dilate the pupils. Mice were placed on a heating pad inside of a Faraday cage directly in front of the desktop BigShot LED Ganzfeld stimulator (LKC Technologies, Gaithersburg, MD, USA). Custom-made platinum wire fiber electrodes were placed in contact with each individual cornea. Refresh tears (Allergan) were added to form a "bubble" on each eye in order to maintain conductivity with the electrode fibers. The 1-centimeter reference electrodes (LKC Technologies) were inserted into each cheek pad and a ground electrode (LKC Technologies) was placed in the tail. ERGs were recorded for the scotopic condition (0.00039–137 cd s/m^2 with 3–10 flash stimuli increasing in time intervals ranging from 4.1 to 62.6 seconds) and for the photopic condition (0.16–79.65 cd s/m^2 with 25 flash stimuli at time intervals of 0.476 seconds). Afterward, mice were injected with reversal agent (0.5 mg/mL atipamezole, injection volume 5 µL per gram mouse weight; Patterson Veterinary) and placed individually in cages on top of heated water pads until fully awake.

In Vivo Ocular Imaging

Mice were anesthetized using IP injections of 100 mg/kg of ketamine and 15 mg/kg xylazine as above. Once anesthetized, proparacaine and tropicamide eye drops were administered as a topical anesthetic and to dilate the pupils as above. A MicronIV spectral domain optical coherence tomography (SD-OCT) system with fundus camera (Phoenix Research Labs, Pleasanton, CA, USA) was used to obtain fundus photographs and retinal morphology for both eyes. Images were taken after clear visualization of the fundus with the optic nerve centered was obtained. Circular SD-OCT B-scans approximately 100 micrometers from the optic nerve head were taken and 50 scans were averaged together. The retinal morphology images were analyzed for both total retinal thickness and photoreceptor layer thickness using Photoshop CS6 (Adobe Systems Inc., San Jose, CA, USA) by two individuals who were masked to sample identity. The number of pixels was converted into micrometers by multiplying by a conversion factor (1 pixel = 1.3 micrometer).

Afterward, a rigid contact lens was placed on the eye (BOZR = 1.7 mm, diameter = 3.2 mm, power = Plano), and confocal scanning laser ophthalmoscopy (cSLO) blue autofluorescence (488 nm excitation wavelength) imaging was conducted using the Spectralis HRA + OCT (Heidelberg Engineering) instrument. Various images were taken

Table. Sample Sizes for Each Group Per Technique

	ERG	Fundus and SD-OCT Images	HRA cSLO	Eye Weights	H&E
Group 1	$N = 10$	$N = 13$	$N = 12$	$N = 10$	$N = 4$
	F = 3; M = 7	F = 3; M = 10	F = 4; M = 8	F = 3; M = 7	F = 2; M = 2
Group 2	$N = 7$	$N = 12$	$N = 11$	$N = 4$	$N = 3$
	F = 6; M = 1	F = 3; M = 9	F = 5; M = 6	F = 4; M = 0	F = 1; M = 2
Group 3	$N = 5$	$N = 9$	$N = 10$	$N = 6$	$N = 4$
	F = 2; M = 3	F = 6; M = 3	F = 8; M = 2	F = 4; M = 2	F = 3; M = 1
Group 4	$N = 3$	$N = 8$	$N = 5$	$N = 6$	$N = 3$
	F = 3; M = 0	F = 4; M = 4	F = 2; M = 3	F = 3; M = 3	F = 1; M = 2

Investigative Ophthalmology & Visual Science

en face at fairly discrete depths using intraocular landmarks. For the purposes of this study, we are showing images from the "farthest"/deepest layer, which we believe to be at the level of the photoreceptor-RPE cells. During imaging and anesthetic recovery, the mice were kept on water-circulating heat pads to maintain their body temperature.

Ocular Section Histology

Eyes were enucleated and placed in 10 mL of chilled 95% methanol 5% acetic acid for 4 days at −80°C. Afterward, samples were dehydrated twice in 100% ethanol for 20 minutes, placed in xylene twice for 20 minutes, and then embedded in paraffin. Sagittal plane sections were cut at 5 micrometer increments. Sagittal sections containing the optic nerve were selected for further staining to ensure consistency across all samples. Sections were then stained with hematoxylin and eosin (H&E) to visualize retinal morphology. Nuclei in the ONL, INL, and GCL were counted manually by two individuals who were masked to sample identity. Only nuclei within a 100-micrometer section were counted using Photoshop CS6 at regularly spaced intervals 250 micrometers apart from the optic nerve in both the superior and inferior directions.

Eye and Body Weight

Mouse body-weight measurements were taken using a scale (Escali Corporation Model L600, Burnsville, MN, USA). Eyes were enucleated and fat and extra ocular muscle were removed using forceps under a dissecting microscope. Individual eyes were then weighed (Denver Instrument Company Model A-160, Bohemia, NY, USA).

Statistical Analysis

Statistical analysis was conducted using Prism 8.4.2 on Mac OS X Version 7 (GraphPad Software, Inc., La Jolla, CA, USA). All data are summarized as mean +/− standard deviation (SD) and individual statistical tests are listed in figure legends. Any P values < 0.05 were considered to be statistically significant. Each sample group member is an independent mouse and sample sizes for each figure are listed in the Table.

Results

We first assessed how retinal function changes with age by recording a- and b-waves in both scotopic and photopic conditions across a series of increasing flash intensities. Overall, both bar and line graphs of a- and b-wave amplitudes showed significant decreases in retinal function across different age groups regardless of condition (Supplementary Fig. S1). These differences were most evident when looking at the raw average ERG waveforms from the youngest animals (group 1) and the oldest animals (group 4; Supplementary Fig. S2). At low flash intensities in both scotopic and photopic conditions, there was little difference between the two groups; however, at medium and high flash intensities in both scotopic and photopic conditions, the differences became much more apparent. At the highest flash intensities (137 cd s/m^2 for scotopic conditions or 79.65 cd s/m^2 for photopic conditions), there were significant differences among the youngest group (group 1) and the three older groups (group 2, group 3, and group 4; Fig. 1). There were significant differences among group 1 and the remaining

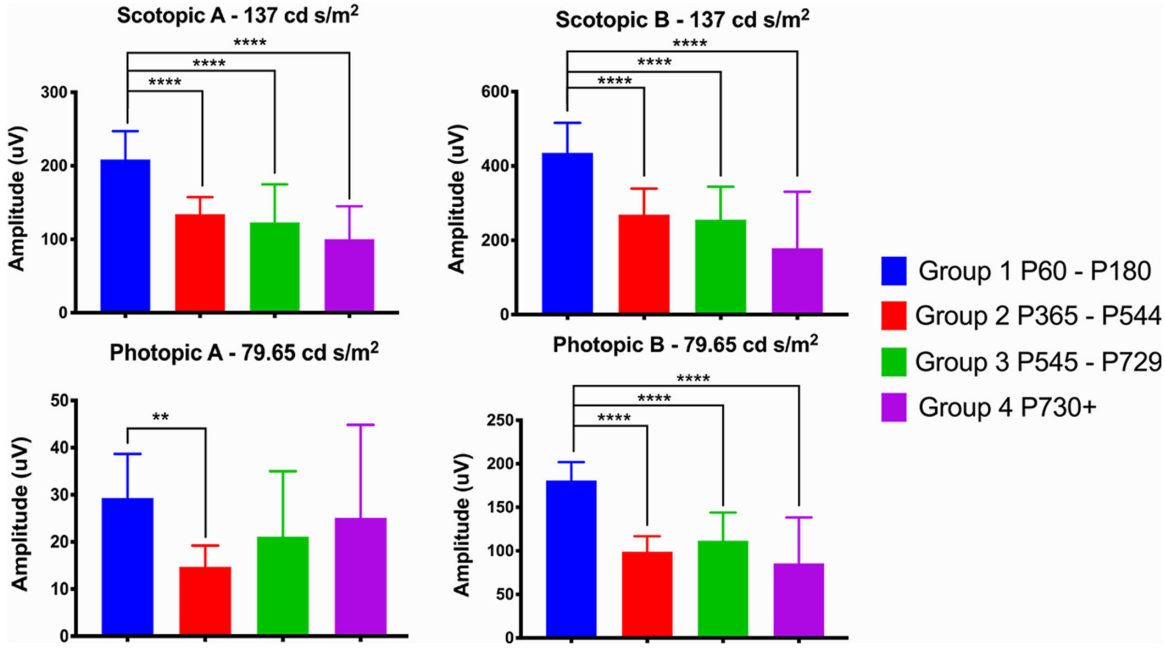

Figure 1. Electroretinogram recordings of a- and b-waves show decreased retinal function in both scotopic and photopic conditions as age increases. Bar graphs show the amplitude of a-waves and b-waves for both scotopic conditions and photopic conditions at the highest flash intensities (137 cd s/m^2 or 79.65 cd s/m^2, respectively). In all four conditions, there are significant decreases in retinal function as age increases. For scotopic a-waves, there are significant differences among group 1 and the remaining three groups (group 2, group 3, and group 4). No differences were observed among group 2, group 3, and group 4. The same pattern is observed for the scotopic b-waves, photopic a-waves, and photopic b-waves. A 2-way ANOVA with Tukey's multiple comparisons test was conducted between the mean amplitudes in all possible pair combinations across all four conditions. A full list of comparisons and P values is listed in Supplementary Figure S1 and Supplementary Tables S1 to S4. Sample sizes Group 1 (< 0.5 years) $n = 10$ (3F/7M); group 2 (1.0–1.5 years) $n = 7$ (6F/1M); group 3 (1.5–2.0 years) $n = 5$ (2F/3M); group 4 (> 2.0 years) $n = 3$ (3F). * = P value < 0.05; ** = P value < 0.01; *** = P value < 0.001; **** = P value < 0.0001.

Investigative Ophthalmology & Visual Science

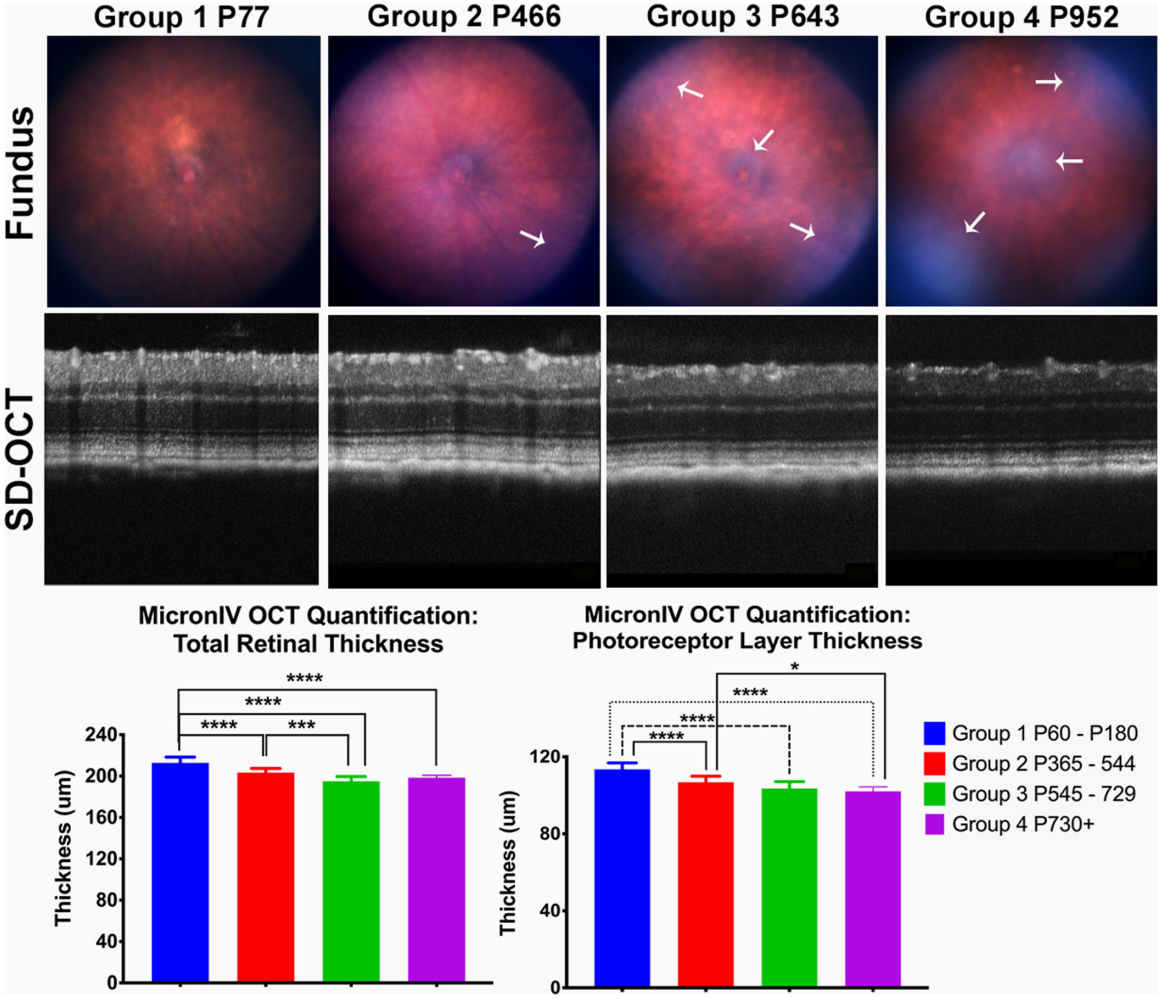

Figure 2. *In vivo* imaging of C57BL/6J retinas shown significant decreases in total retinal thickness and photoreceptor layer thickness over time. SD-OCT images show total retinal thickness and photoreceptor layer thickness decrease over time. Micron IV fundus photography shows an increased mottled or dappled appearance in C57BL/6J eyes with aging (additional images available in Supplementary Fig. S2). There are also opacities and uneven illumination evident in the older animals that could be indicative of increased cataract development or incomplete iris dilation. These features have been highlighted by *white arrows*. *Green circles* indicate the circumference where retinal b-scans were taken from. Scans did not cut through any features indicated by the *white arrows*. Additionally, quantification of SD-OCT images, circular scans taken approximately 100 micrometers from the optic nerve head, show a significant decrease in total retinal thickness among group 1 and group 2, group 3 and group 4. There was also a significant decrease in total retinal thickness between group 2 and group 3. When specifically looking at the ONL (photoreceptor layer), a significant decrease was observed among group 1 and group 2, group 3 and group 4 as well as between group 2 and group 4. A 1-way ANOVA with Tukey's multiple comparisons test was conducted between the mean thickness measurements in all possible pair combinations. A full list of comparisons and *P* values is listed in Supplementary Table S5 (Total Retinal Thickness) or Supplementary Table S6 (Total Photoreceptor Layer Thickness). Sample sizes group 1 (< 0.5 years) $n = 13$ (3F/10M); group 2 (1.0–1.5 years) $n = 12$ (3F/9M); group 3 (1.5–2.0 years) $n = 9$ (6F/3M); and group 4 (> 2.0 years) $n = 8$ (4F/4M). * = *P* value < 0.05; ** = *P* value < 0.01; *** = *P* value < 0.001; **** = *P* value < 0.0001.

three groups (group 2, group 3, and group 4) in the scotopic a-wave. No differences were observed among group 2, group 3, and group 4. The same pattern was observed for the scotopic b-waves and photopic b-waves. Photopic a-waves only showed significant differences between group 1 and group 2, not among the older groups. The full list of statistical comparisons for a- and b-wave ERG results in both scotopic and photopic conditions at increasing flash intensities is available in Supplementary Tables S1 to S4.

Morphological changes were seen with age in fundus and SD-OCT images. Qualitatively, as age increases, there was an increasingly mottled appearance in the C57BL/6J fundus photographs (Supplementary Fig. S3). Additionally, there are also opacities evident in the older animals that could be indicative of increased cataract development or complications of incomplete iris dilation. We have highlighted some, but not all, of these features with white arrows in both Figure 2 and Supplemental Figure S3. Quantification of the total retinal thickness and ONL from SD-OCT images showed significant decreases as age increased (see Fig. 2). For total retinal thickness, there were significant decreases among group 1 and the remaining three groups (group 2, group 3, and group 4). There was also a significant decrease in total retinal thickness between group 2 and group 3. When specifically looking at the ONL, a significant decrease was observed among group 1 and the remaining groups (group 2, group 3, and group 4) as well as between group 2 and group 4. A full list of statistical comparisons for total retinal

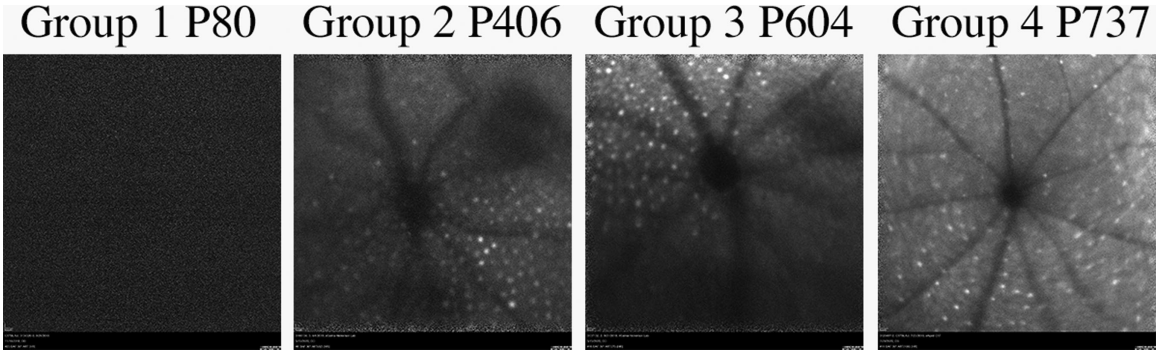

Figure 3. Heidelberg Spectralis cSLO images show increased blue auto-fluorescence at the photoreceptor-RPE junction as age increases. Sample sizes group 1 (< 0.5 years) $n = 12$ (4F/8M); group 2 (1.0–1.5 years) $n = 11$ (5F/6M); group 3 (1.5–2.0 years) $n = 10$ (8F/2M); and group 4 (> 2.0 years) $n = 5$ (2F/3M).

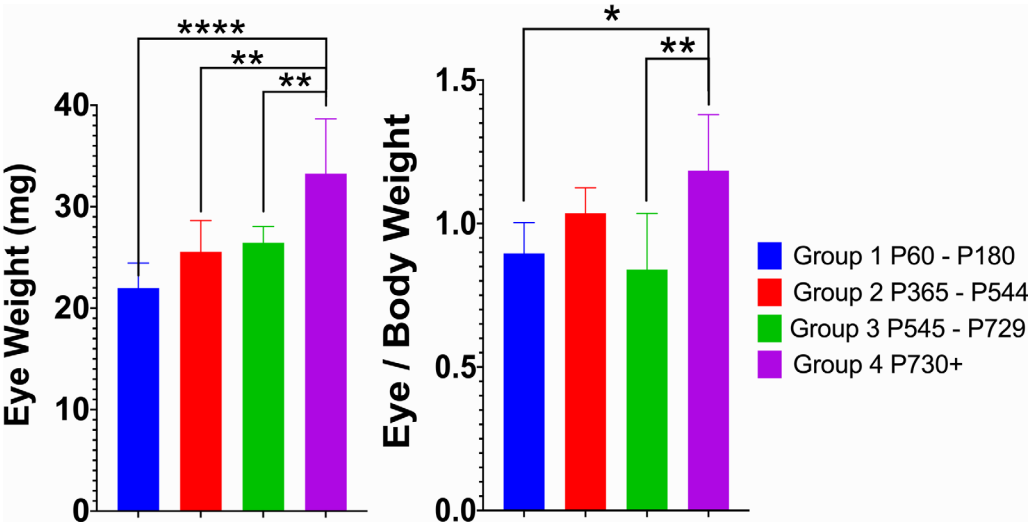

Figure 4. Eye weights increase with age. Raw eye weight data show a gradual and significant increase between group 1 and group 4, group 2 and group 4, and group 3 and group 4. When the eye weight is adjusted for the body weight of the animal, there remains a significant difference between group 1 and group 4 as well as group 3 and group 4. Sample sizes group 1 (< 0.5 years) $n = 10$ (3F/7M); group 2 (1.0–1.5 years) $n = 4$ (4F); group 3 (1.5–2.0 years) $n = 6$ (4F/2M); and group 4 (> 2.0 years) $n = 6$ (3F/3M). * = P value < 0.05; ** = P value < 0.01; *** = P value < 0.001; **** = P value < 0.0001.

thickness and photoreceptor layer thickness is available in Supplementary Tables S5 and S6, respectively.

In addition to the thickness changes seen in the retina, changes were also observed in representative cSLO images from the layer of cells at the general level of the photoreceptor-RPE interface (Fig. 3, Supplementary Fig. S4). These images capture the area from the external limiting membrane through the inner and outer segments and continues through the interdigitations between the outer segments and RPE cells into the apical face of the RPE. In the youngest animals (group 1), no abnormalities were observed in the fundus autofluorescence images; however, numerous discrete small punctate spots became apparent by one year of age (group 2) and remained constant and pronounced up to 2+ years of age (group 4).

After ERGs and *in vivo* images were collected, the eyes were enucleated and weighed. Eye weights increased gradually, but significantly with age among group 1 and the remaining three groups (group 2, group 3, and group 4; Fig. 4). However, when the eye weight is adjusted for the body weight of the animal, there is only a significant difference between group 1 and group 4, and between group 3 and group 4. A full list of statistical comparisons for eye weight and eye weight adjusted for body weight is available in Supplementary Tables S7 and S8, respectively.

Finally, H&E staining provided a more detailed overview of the morphological changes that occur during aging. We show one representative whole eye, retina, and photoreceptor–RPE interface image for each group (Fig. 5). Overall, we did not observe any obvious morphological changes in the retina as age increases. In group 4, there were some subtle irregularities in the inner and outer segments and the RPE sheet was slightly bumpy with small amounts of irregular thinning and elevation in patches, which we hypothesize to correspond with the mottling that was observed in the fundus images (Supplementary Fig. S5). Alas, we are unable to prove or disprove this hypothesis until better alignment and registration can be achieved. Quantification of cell nuclei number at 250 micrometer intervals from the optic nerve head both in the superior and inferior direction for the ONL, INL, and GCL showed consistent significant decreases in the ONL, but not the

Investigative Ophthalmology & Visual Science

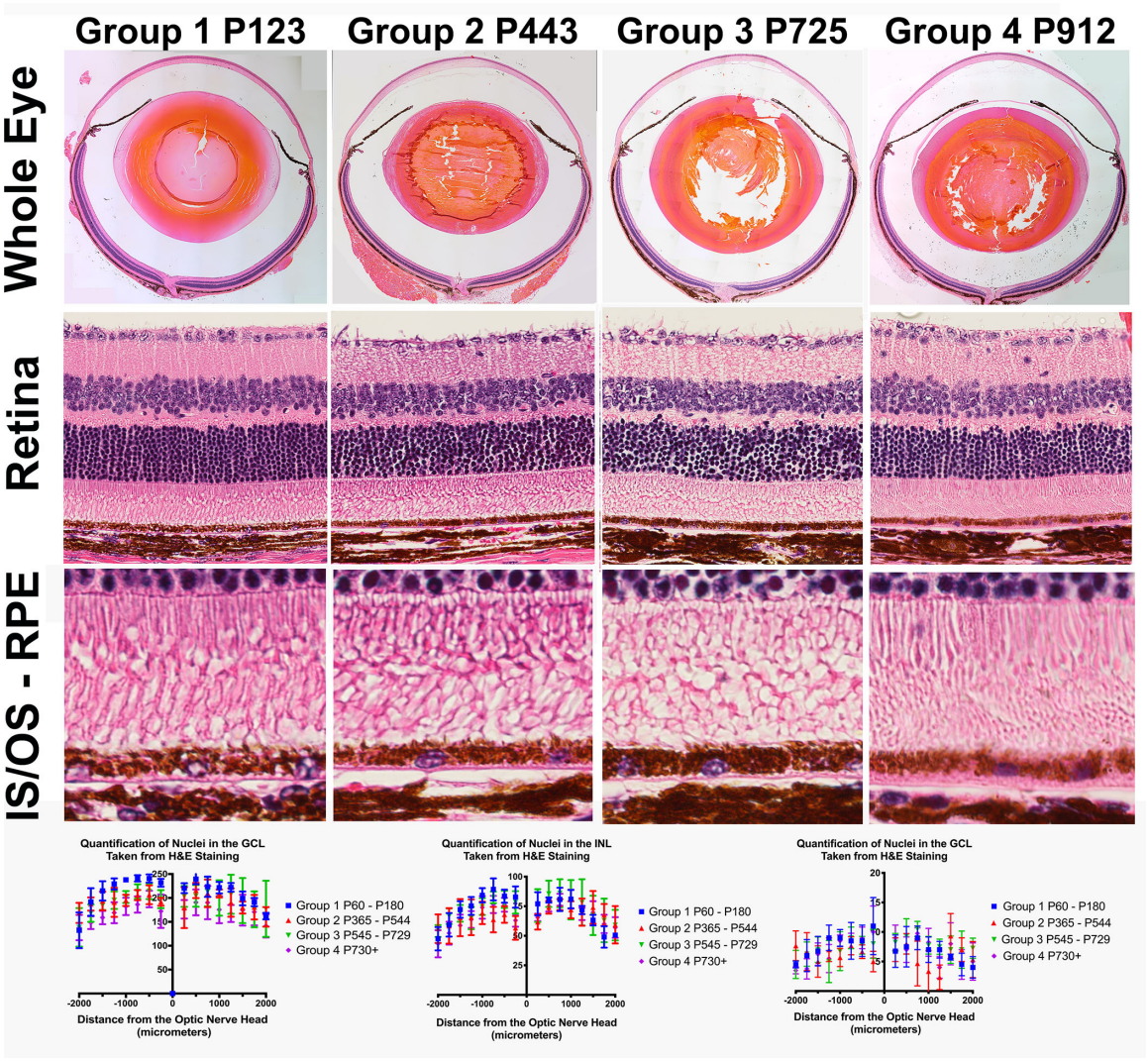

Figure 5. Post mortem retinal morphology shows decreasing cell nuclei counts in the outer nuclear layer (ONL) with increasing age whereas inner nuclear layer (INL) and ganglion cell layer (GCL) remain relatively equal. Representative images of H&E staining of the whole eye and retinal sections from all four groups shows gross changes in retinal morphology. Quantification of cell nuclei counts at 250-micrometer intervals from the optic nerve head both in the superior and inferior direction in the ONL show statistically significant decreases between group 1 and group 4 at the majority of the intervals: however, no significant differences among group 1, group 2, and group 3. A 2-way ANOVA with Tukey's multiple comparisons test was conducted between the mean nuclei counts in all possible pair combinations. A full list of comparisons and *P* values is listed for the ONL, INL, and GCL in Supplementary Tables S9 to S11, respectively. Total sample sizes for H&E-stained images: group 1 (< 0.5 years) $n = 4$ (2F/2M); group 2 (1.0–1.5 years) $n = 3$ (1F/2M); group 3 (1.5–2.0 years) $n = 4$ (3F/1M); and group 4 (> 2.0 years) $n = 3$ (1F/2M). * = *P* value < 0.05; ** = *P* value < 0.01; *** = *P* value < 0.001; **** = *P* value < 0.0001.

INL or GCL (see Fig. 5). In the ONL, there were significant decreases in the number of nuclei at the majority of intervals between group 1 and group 4; however, no significant differences were observed among group 1, group 2 and group 3. In the INL and GCL, whereas there were certain intervals that had significant decreases, they were not consistent among particular groups or at particular intervals. Therefore, they were likely not biologically meaningful. We also quantified the RPE thickness and number of cells in the subretinal space; however, there were no significant differences between any of the groups (Supplementary Fig. S5). A full list of statistical comparisons for nuclei counts in the ONL, INL, and GCL is available in Supplementary Tables S9 to S11, respectively. Additionally, statistical comparisons for RPE thickness across age and the number of cells in the subretinal space are available in Supplementary Tables S12 to S14.

Discussion

The purpose of this study was to expand our current understanding of how natural aging affects retinal function and morphology. Here, we sought to understand if vision changes due to natural aging occur gradually or abruptly. Whereas the majority of aging studies in the visual system compare one "young" group of animals to another "old" group, one that is generally 1 to 2 years old, our study has multiple age groups and extends the upper age limit of our animals to approximately 2.65 years (P970). Although the relationship between mouse and human age is not directly

Investigative Ophthalmology & Visual Science

correlated due to developmental differences, the upper age limit of 2.65 years for mice is close to the maximum life expectancy of a laboratory mouse and thus may represent people who are centenarians (100+ years old) or supercentenarians (110+ years old).[20]

When assessing retinal function through ERGs (see Fig. 1, Supplementary Figs. S1, S2), there were significant differences among the "young" group (< 0.5 years) and the three older groups for scotopic a- and b-waves and photopic b-waves. Photopic a-waves only showed significant differences between group 1 and group 2, not with the older groups. This is likely due to the large variation in responses in older animals, suggesting that cone functionality may be more sensitive and variable in aging compared to rod photoreceptors or the inner retinal neurons. Additionally, cone photoreceptors make up a very small percentage of mouse retinal neurons (< 3%); therefore, small differences in cone death or dysfunction in individual mice could have a large impact on the group's variation.

When assessing retinal morphology through SD-OCT and fundus images (see Fig. 2, Supplementary Fig. S3), the fundus images show a clear increase in mottling with age. This mottling may be due to a number of different causes, including, but not limited to, the loss and/or reorganization of RPE cells or changes in the structures underneath the retina, including the subretinal space, RPE, or choroid. The exact cause of the mottling is beyond the scope of this present study but should be noted. The SD-OCT images show gradual and significant decreases in total retinal thickness and photoreceptor layer thickness. For total retinal thickness, there were significant decreases among group 1 and the remaining three age groups, but also between group 2 and group 3. This suggests that between the ages of 2 months and 2 years, there was likely a loss of neuronal cell bodies or synapses; however, after 2 years of age, the total retinal thickness stabilizes. The ONL followed a similar trend where the thickness significantly decreased among group 1 and the remaining three age groups. Additionally, significant differences were also seen between groups 2 and 4, not groups 2 and 3, suggesting that the overall ONL thickness stabilized across 1 year of age, but then decreased again at 2 years of age. One technical limitation in our SD-OCT image methodology is that our images are obtained from a ring approximately 100 micrometers from the optic nerve head. Therefore, any changes outside of this immediate area, including those in peripheral areas as well as those in the nasal-temporal or equatorial orientations would be missed. Age-related increases in mottling and lens opacities were observed in fundus images. The white/blue opacities could be indicative of increased cataract formation or due to incomplete iris dilation. Changes in the clarity of the optical media, whether via corneal opacity, lens opacity, or any other disturbances, will lead to a scattering of light. Less light hitting the back of the eye will reduce the intensity of the fundus, SD-OCT, and auto fluorescence images, and may contribute to a reduction in contrast and detail in the images, including gray spots on the color fundus photographs or "dark" areas on the autofluorescent images.

The cSLO data also showed increased optical aberrations in the blue–autofluorescence among group 1 and the remaining three older groups. These aberrations remained relatively stable after 1 year of age (see Fig. 3, Supplementary Fig. S4). Within a given eye, the aberrations were consistent and remain in the same location even during repeated observation, indicating that they are not artifacts of the instrumentation or the orientation of the mouse's optical axis relative to the instrument's optical axis.

Although our study cannot definitively identify the aberrations, there are multiple hypotheses within the field. The autofluorescent aberrations observed in the cSLO images could be photoreceptor cell rosettes/tubulations resulting from age-related degeneration of the ONL.[21] These ONL tubulations have been previously observed in patients with age-related macular degeneration (AMD).[22] The retinal degeneration can lead to the accumulation of bisretinoid compounds that are transferred to the RPE during photoreceptor outer segment membrane shedding and phagocytosis.[23,24] This intracellular lipofuscin is a hallmark of aging[25] and contains fluorophores, such as A2E.[26,27] Lipofuscin accumulation is mostly observed in many different retinal degeneration and detachment animal models[28–30] and can be quantified *in vivo*.[31] Commercially available C57BL/6N mice have been found with *rd8* mutations, resulting in retinal degeneration and confounding interpretations.[32] Our animals were purchased from Jackson Laboratories (C57BL/6J) and were screened for *rd8* mutations. None of our animals had *rd8* mutations and we do not observe any photoreceptor rosettes in the H&E sections; therefore, we view the degeneration hypothesis less favorably.

Another possible source of the autofluorescence are microglia. Microglia have numerous roles in both healthy and degenerating eyes.[33–35] We hypothesize that some of the autofluorescence may be contributed by surveilling and activated microglia that phagocytosed cellular debris, including lipofuscin. The interplay among A2E, lipofuscin, and subretinal microglia activation and accumulation has been extensively studied and can cause AMD-like features in transgenic mouse models.[36–40] Autofluorescent granule deposits have been observed in Iba1+ positive microglia found in both the perivasculature and subretinal space in 12- and 18-month old mice.[41] This increase in microglial presence corresponds with changes in gene expression related to immune activation in the aging retina.[42,43] Although these microglia and macrophages are active in aged wildtype and transgenic mouse models, there is little evidence to support their presence in aged human RPE or AMD-related subretinal drusen deposits.[44,45] Overall, the lack of rosettes in H&E sections and outer retinal tubulations in the SD-OCT imaging seems to eliminate those two possibilities and favor the microglia and macrophage hypothesis; however, our data do not firmly establish the identity of the aberrations. This will require future experimentation.

A technical limitation that may contribute to the sudden increase in autofluorescence in the cSLO images among group 1 and the remaining groups is automatic normalization by the Spectralis software. The Spectralis equipment normalizes the overall intensity of different cSLO images; therefore, as fluorescent agents accumulate with increasing age, a threshold of fluorescence will be reached that the equipment can detect and produce an image with sufficient detail. This can make intensity comparisons between individual mice and different ages difficult to interpret. Another limitation is that the automatic normalization and variation in optical media clarity between different eyes leads to variable image quality, making quantitative assessment of fluorescent intensities difficult.

The changes seen in lens opacity corroborated eye weight data, which showed increasing eye weight as age increases, even when adjusted for the body weight of the individual mouse (see Fig. 4). The lens continuously grows throughout

life when new epithelial cells differentiate into fiber cells and then lay down over existing cells to form distinctive layers.[46]

Finally, cell nuclei quantification taken from H&E-stained sagittal cross-sections of the retina showed significant decreases in the ONL, but not in the INL or GCL, between group 1 and group 4 at the majority of the intervals (see Fig. 5). There were no significant differences among group 1, group 2 and group 3. This differs from observations by *in vivo* SD-OCT imaging, where differences among group 1 and the other three groups were observed in the ONL. This discrepancy is likely due to the cell nuclei counts being done within 100 micrometer sections along the length of the entire retina in contrast to the OCT images, which were taken at a central area near the optic nerve head. There were also no significant differences in the RPE thickness or number of cells in the subretinal space across age, although some RPE irregularities were observed (see Supplementary Fig. S5).

Aging is a biological process that affects all organ systems, tissues, and cell types and factors, such as genetics, nutrition, and physical activity can modulate its effects on health.[47] Aging affects different biological processes, such as mitochondrial function, proteostasis, autophagy, and cellular senescence via alterations in genomic stability, epigenetics, and transcription.[48–52] Resources, such as the Age Phenome Knowledgebase, and animal models of aging highlight how this process affects all organ systems and tissues, including the eyes.[53,54] Age remains one of the major risk factors for various ophthalmic disorders, most notably cataracts, glaucoma, and AMD.[55–57] Yet, despite this vast wealth in knowledge, there is little information about the rate of vision loss over time or how specific biological processes affect the rate of visual decline. Overall, our study aligns with and builds upon previous literature studying the effects of aging on the visual system. One limitation of our study is our focus on only one mouse strain, C57BL/6J. Although these highly inbred mice are considered "wild-type" and many genetic mutant strains are made or studied on this background, there are many other "wild-type" inbred mouse strains that represent substantially different genetic backgrounds. Thus, the changes that we observed may be specific to a particular genetic background and will likely be influenced by allelic or single nucleotide polymorphism (SNP) differences that are unique to that particular strain. Another limitation in this current study is our focus on the retina only, not on other ocular tissues, such as the cornea or RPE, which are also known to undergo natural changes related to aging. Specifically, in AMD, the RPE becomes dysfunctional and is no longer able to perform its synergistic role in nourishing and protecting photoreceptors. In addition to this synergistic role, the RPE also performs other critical functions, including forming the blood-retina barrier, transporting nutrients, retinoids, and waste products and phagocytosis of outer segments.[58] Future studies need to assess the natural effects of aging on these structures, especially at the extreme ages (2+ years) that represent the upper limit of life expectancy.

Acknowledgments

Supported by National Institutes of Health (NIH) grants R01EY028450, R01EY021592, P30EY006360, F31EY028855, R01EY028859, T32EY07092, and T32GM008490, the Abraham and Phyllis Katz Foundation, VA RR&D I01RX002806 and I21RX001924, VA RR&D C9246C (Atlanta Veterans Administration Center for Excellence in Vision and Neurocognitive Rehabilitation), and an unrestricted grant to the Department of Ophthalmology at Emory University from Research to Prevent Blindness, Inc.

Disclosure: **S. Ferdous,** None; **K.L. Liao,** None; **I.D. Gefke,** None; **V.R. Summers,** None; **W. Wu,** None; **K.J. Donaldson,** None; **Y.-K. Kim,** None; **J.T. Sellers,** None; **J.A. Dixon,** None; **D.A. Shelton,** None; **S. Markand,** None; **S.M. Kim,** None; **N. Zhang,** None; **J.H. Boatright,** None; **J.M. Nickerson,** None

References

1. Swenor BK, Lee MJ, Varadaraj V, Whitson HE, Ramulu PY. Aging with vision loss: a framework for assessing the impact of visual impairment on older adults. *Gerontologist*. 2020;60(6):989–995.
2. Lin JB, Tsubota K, Apte RS. A glimpse at the aging eye. *NPJ Aging Mech Dis*. 2016;2(1):1–7.
3. Ryoo NK, Ahn SJ, Park KH, et al. Thickness of retina and choroid in the elderly population and its association with Complement Factor H polymorphism: KLoSHA Eye study. *PLoS One*. 2018;13(12):1–15.
4. Chauhan BC, Vianna JR, Sharpe GP, et al. Differential effects of aging in the macular retinal layers, neuroretinal rim and peripapillary retinal nerve fibre layer. *Ophthalmology*. 2020;127(2):177–185.
5. Curcio CA, Millican CL, Allen KA, Kalina RE. Aging of the human photoreceptor mosaic: Evidence for selective vulnerability of rods in central retina. *Investig Ophthalmol Vis Sci*. 1993;34(12):3278–3296.
6. Lin Y, Jiang H, Liu Y, et al. Age-related alterations in retinal tissue perfusion and volumetric vessel density. *Investig Ophthalmol Vis Sci*. 2019;60(2):685–693.
7. Orlov N V., Coletta C, van Asten F, et al. Age-related changes of the retinal microvasculature. *PLoS One*. 2019;14(5):1–17.
8. Eells JT. Mitochondrial dysfunction in the aging retina. *Biology (Basel)*. 2019;8(2):31.
9. Xu H, Chen M, Forrester J V. Para-inflammation in the aging retina. *Prog Retin Eye Res*. 2009;28(5):348–368.
10. Birch DG, Anderson J. Standardized full-field electroretinography. *Arch Ophthalmol*. 1992;110:1571–1576.
11. Weleber RG. The effect of age on human cone and rod ganzfeld electroretinograms. *Investig Ophthalmol Vis Sci*. 1981;20(3):392–399.
12. Damani MR, Zhao L, Fontainhas AM, Amaral J, Fariss RN, Wong WT. Age-related alterations in the dynamic behavior of microglia. *Aging Cell*. 2008;10(2):263–276.
13. Telegina D V., Kozhevnikova OS, Kolosova NG. Changes in retinal glial cells with age and during development of age-related macular degeneration. *Biochem*. 2018;83(9):1009–1017.
14. Tarau I-S, Berlin A, Curcio CA, Ach T. The cytoskeleton of the retinal pigment epithelium: from normal aging to age-related macular degeneration. *Int J Mol Sci*. 2019;20(14):3578.
15. Delori C, Goger DG, Dorey CK. Age-related accumulation and spatial distribution of lipofuscin in RPE of normal subjects. *Invest Ophthalmol Vis Sci*. 2001;42(8):1855–1866.
16. Presley JB, Chimento MF, Curcio CA. Comparison of morphology of human macular and peripheral Bruch's membrane in older eyes. *Curr Eye Res*. 2008;32(9):791–799.
17. Nadal-Nicolás FM, Vidal-Sanz M, Agudo-Barriuso M. The aging rat retina: from function to anatomy. *Neurobiol Aging*. 2018;61:146–168.
18. Cano J, Machado A, Reinoso-Suárez F. Morphological changes in the retina of ageing rats. *Arch Gerontol Geriatr*. 1986;5(1):41–50.
19. Wang Y, Grenell A, Zhong F, et al. Metabolic signature of the aging eye in mice. *Neurobiol Aging*. 2018;71:223–233.

20. Dutta S, Sengupta P. Men and mice: Relating their ages. *Life Sci*. 2016;152:244–248.
21. Flynn E, Ueda K, Auran E, Sullivan JM, Sparrow JR. Fundus autofluorescence and photoreceptor cell rosettes in mouse models. *Investig Ophthalmol Vis Sci*. 2014;55(9):5643–5652.
22. Schaal KB, Freund KB, Litts KM, Zhang Y, Messinger JD, Curcio CA. Outer retinal tubulation in advanced age-related macular degeneration: optical coherence tomographic findings correspond to histology. *Retina*. 2015;35(7):1339–1350.
23. Sparrow JR, Yoon KD, Wu Y, Yamamoto K. Interpretations of fundus autofluorescence from studies of the bisretinoids of the retina. *Investig Ophthalmol Vis Sci*. 2010;51(9):4351–4357.
24. Secondi R, Kong J, Blonska AM, Staurenghi G, Sparrow JR. Fundus autofluorescence findings in a mouse model of retinal detachment. *Investig Ophthalmol Vis Sci*. 2012;53(9):5190–5197.
25. Shrehler B, Mark D, Mildvan A. Rate and magnitude of age pigment accumulation in the human myocardium. *J Gerontol*. 1959;14:430–439.
26. Ben-Shabat S, Parish CA, Vollmer HR, et al. Biosynthetic studies of A2E, a major fluorophore of retinal pigment epithelial lipofusein. *J Biol Chem*. 2002;277(9):7183–7190.
27. Sparrow JR, Kim SR, Wu Y. Experimental approaches to the study of A2E, a bisretinoid lipofuscin chromophore of retinal pigment epithelium. *Methods Mol Biol*. 2010;652:315–327.
28. Mata NL, Weng J, Travis GH. Biosynthesis of a major lipofuscin fluorophore in mice and humans with ABCR-mediated retinal and macular degeneration. *Proc Natl Acad Sci USA*. 2000;97(13):7154–7159.
29. Ambati J, Anand A, Fernandez S, et al. An animal model of age-related macular degeneration in senescent Ccl-2- or Ccr-2-deficient mice. *Nat Med*. 2003;9(11):1390–1397.
30. Wang NK, Fine HF, Chang S, et al. Cellular origin of fundus autofluorescence in patients and mice with a defective NR2E3 gene. *Br J Ophthalmol*. 2009;93(9):1234–1240.
31. Nafar Z, Wen R, Guan Z, Li Y, Jiao S. Quantifying lipofuscin in retinal pigment epithelium *in vivo* by visible-light optical coherence tomography-based multimodal imaging. *Sci Rep*. 2020;10(1):1–10.
32. Mattapallil MJ, Wawrousek EF, Chan CC, et al. The Rd8 mutation of the Crb1 gene is present in vendor lines of C57BL/6N mice and embryonic stem cells, and confounds ocular induced mutant phenotypes. *Invest Ophthalmol Vis Sci*. 2012;53(6):2921–2927.
33. Chen L, Yang P, Kijlstra A. Distribution, markers, and functions of retinal microglia. *Ocul Immunol Inflamm*. 2002;10(1):27–39.
34. Karlstetter M, Ebert S, Langmann T. Microglia in the healthy and degenerating retina: Insights from novel mouse models. *Immunobiology*. 2010;215(9-10):685–691.
35. Karlstetter M, Scholz R, Rutar M, Wong WT, Provis JM, Langmann T. Retinal microglia: Just bystander or target for therapy? *Prog Retin Eye Res*. 2015;45:30–57.
36. Combadière C, Feumi C, Raoul W, et al. CX3CR1-dependent subretinal microglia cell accumulation is associated with cardinal features of age-related macular degeneration. *J Clin Invest*. 2007;117(10):2920–2928.
37. Raoul W, Feumi C, Keller N, et al. Lipid-bloated subretinal microglial cells are at the origin of drusen appearance in CX3CR1-deficient mice. *Ophthalmic Res*. 2008;40(3-4):115–119.
38. Luhmann UFO, Robbie S, Munro PMG, et al. The drusen-like phenotype in aging Ccl2-knockout mice is caused by an accelerated accumulation of swollen autofluorescent subretinal macrophages. *Investig Ophthalmol Vis Sci*. 2009;50(12):5934–5943.
39. Chinnery HR, McLenachan S, Humphries T, et al. Accumulation of murine subretinal macrophages: Effects of age, pigmentation and CX 3CR1. *Neurobiol Aging*. 2012;33(8):1769–1776.
40. Ma W, Coon S, Zhao L, Fariss RN, Wong WT. A2E accumulation influences retinal microglial activation and complement regulation. *Neurobiol Aging*. 2013;34(3):943–960.
41. Xu H, Chen M, Manivannan A, Lois N, Forrester J V. Age-dependent accumulation of lipofuscin in perivascular and subretinal microglia in experimental mice. *Aging Cell*. 2008;7(1):58–68.
42. Yoshida S, Yashar BM, Hiriyanna S, Swaroop A. Microarray analysis of gene expression in the aging human retina. *Investig Ophthalmol Vis Sci*. 2002;43(8):2554–2560.
43. Chen M, Muckersie E, Forrester J V., Xu H. Immune activation in retinal aging: A gene expression study. *Investig Ophthalmol Vis Sci*. 2010;51(11):5888–5896.
44. Ach T, Huisingh C, McGwin G, et al. Quantitative autofluorescence and cell density maps of the human retinal pigment epithelium. *Investig Ophthalmol Vis Sci*. 2014;55(8):4832–4841.
45. Chen L, Messinger JD, Zhang Y, Spaide RF, Freund KB, Curcio CA. Subretinal drusenoid deposit in age-related macular degeneration: histologic into initiation, progression to atrophy, and imaging. *Retina*. 2020;40(4):618–631.
46. Augusteyn RC. Growth of the eye lens: I. Weight accumulation in multiple species. *Mol Vis*. 2014;20(October 2013):410–426.
47. Partridge L, Deelen J, Slagboom PE. Facing up to the global challenges of ageing. *Nature*. 2018;561(7721):45–56.
48. Ferrucci L, Gonzalez-Freire M, Fabbri E, et al. Measuring biological aging in humans: A quest. *Aging Cell*. 2019;(July):1–21.
49. Pagiatakis C, Musolino E, Gornati R, Bernardini G, Papait R. Epigenetics of aging and disease: a brief overview [published online ahead of print December 6, 2019]. *Aging Clin Exp Res*, https://do.org/:10.1007/s40520-019-01430-0.
50. López-Otín C, Blasco MA, Partridge L, Serrano M, Kroemer G. The hallmarks of aging. *Cell*. 2013;153(6):1194.
51. Van Deursen JM. The role of senescent cells in ageing. *Nature*. 2014;509(7501):439–446.
52. Wang C, Jurk D, Maddick M, Nelson G, Martin-ruiz C, Von Zglinicki T. DNA damage response and cellular senescence in tissues of aging mice. *Aging Cell*. 2009;8(3):311–323.
53. Mitchell SJ, Scheibye-Knudsen M, Longo DL, de Cabo R. Animal models of aging research: implications for human aging and age-related diseases. *Annu Rev Anim Biosci*. 2015;3(1):283–303.
54. Geifman N, Rubin E. The mouse age phenome knowledgebase and disease-specific inter-species age mapping. *PLoS One*. 2013;8(12):e81114.
55. Lambert NG, Singha MK, ElShelmani H, et al. Risk factors and biomarkers of age-related macular degeneration. *Prog Retin Eye Res*. 2016;54(1):64–102.
56. Al-Zamil WM, Yassin SA. Recent developments in age-related macular degeneration: A review. *Clin Interv Aging*. 2017;12:1313–1330.
57. Chakravarthy U, Wong TY, Fletcher A, et al. Clinical risk factors for age-related macular degeneration: A systematic review and meta-analysis. *BMC Ophthalmol*. 2010;10(1):31.
58. Boulton M, Dayhaw-barker P. The role of the retinal pigment epithelium: topographical variation and ageing changes. *Nature, Eye*. 2001;15:384–389.

Investigative Ophthalmology & Visual Science